THE JOURNAL OF PHYSICAL CHEMISTRY C
A JOURNAL OF THE AMERICAN CHEMICAL SOCIETY

pubs.acs.org/JPCC

Article

Proton Dissociation and Delocalization under Stepwise Hydration of Zeolite HZSM-5

John H. Hack, Xinyou Ma, Yaxin Chen, James P. Dombrowski, Nicholas H. C. Lewis, Chenghan Li, Harold H. Kung, Gregory A. Voth, and Andrei Tokmakoff*

Cite This: *J. Phys. Chem. C* 2023, 127, 16175−16186

Read Online

ACCESS | Metrics & More | Article Recommendations | Supporting Information

ABSTRACT: The protonation behavior of zeolite Brønsted acid sites (BAS) in the presence of water is important for the performance of these widely used catalysts. Despite extensive study, the number of water molecules necessary for deprotonation is not well understood, in large part because experiments have been unable to access this information. In this work, we report experimental evidence for full deprotonation of the BAS in the presence of two or more water molecules, with a deprotonation energy of 1.6 kcal/mol. Linear IR absorption and 2D IR spectra were measured over a wide range of controlled hydration levels from 0.5 to 8.0 equivalents of H_2O/Al at a constant temperature. Distinct spectral signatures of the protonated BAS and excess proton are identified, and their hydration dependence is analyzed quantitatively. Using the experiment as a benchmark, *ab initio* molecular dynamics simulations are reported that reproduce the experimental trends in the protonation state and IR spectra. The proton charge position and delocalization are quantified in clusters of 1−8 H_2O molecules using the recently developed rCEC method. This analysis provides insight into the proton structure in confined water clusters, showing that the excess charge remains relatively localized between two oxygen atoms across the hydration range.

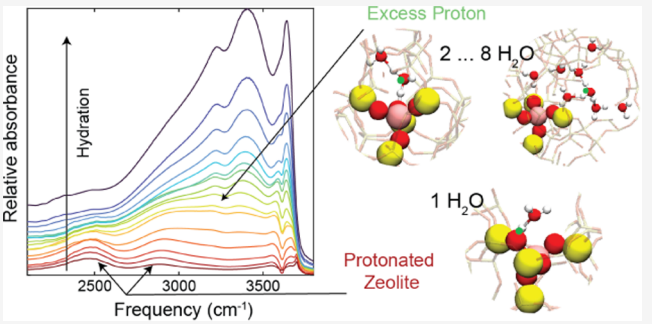

Downloaded via 98.46.108.10 on November 14, 2023 at 03:38:28 (UTC).
See https://pubs.acs.org/sharingguidelines for options on how to legitimately share published articles.

1. INTRODUCTION

Acidic zeolites are among the most widely used heterogeneous catalysts in industrial processes, catalyzing alkylation, isomerization, cracking, and other reactions in oil refining and petrochemistry.[1−4] With the growing need to divest from fossil fuels,[5] zeolites have also emerged as promising catalysts for the production of fuels and chemicals derived from biomass.[6−8] Water is often present as a reaction product or solvent in the conversion of oxygen-rich biomass feedstocks,[9] and has been shown to influence catalytic activity in several zeolite-catalyzed reactions.[10−15] A comprehensive understanding of the protonation state is crucial for gaining a deeper mechanistic understanding of these processes since access to the proton is the basis for the Brønsted acidity of the catalyst.

Despite extensive study, the protonation state of the zeolite Brønsted acid site (BAS) as a function of hydration level is not fully understood. In the presence of a single water molecule, it is well established that the proton resides on the BAS, which donates a H-bond to the adsorbed water molecule.[16−27] The proton affinity of the water cluster increases with size,[28−31] deprotonating the BAS above a critical hydration level. However, the number of water molecules necessary for deprotonation is not known. This has been a topic of many simulation studies, which arrived at different conclusions depending on the computational approach.[17,20−22,24,25,32,33] The main point of debate is the adsorbed water dimer, where different studies concluded that protonated BAS,[22,34] protonated water cluster,[17] or both[20,21,24,25,33] are stable species. To date, experiments that can identify protonation states at distinct microscopic hydration levels have not yet been reported.

Infrared (IR) spectroscopy has been a valuable experimental technique for investigating the hydration behavior of zeolites since the O−H stretch vibrational frequency is sensitive to its molecular H-bonding environment. To date, most IR studies of hydrated zeolite have focused on the characterization of ≤ 1 equivalents (equiv) H_2O/BAS,[16,35−37] where the most prominent spectroscopic feature is a broad doublet arising from the H-bonded BAS O−H stretch.[16,21,38,39] Experimental studies at elevated hydration are more limited. In one approach, the hydration level was controlled by the partial pressure of water vapor in contact with the zeolite, which required calibration to a second gravimetric measurement.[16,40]

Received: May 29, 2023
Revised: July 21, 2023
Published: August 9, 2023

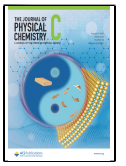

ACS Publications

© 2023 The Authors. Published by American Chemical Society

Alternatively, the water loading was controlled by varying the temperature from 30 to 430 °C,[22] enabling accurate measurement of the hydration level at the cost of temperature effects in the IR spectra. In addition to the experimental challenge of hydration control, quantitative analysis of the protonation state is confounded by broad, overlapping IR features and the inevitable microscopic distribution of hydration states at an average water loading. Notably, a recent ^{1}H NMR study identified a signature of hydronium ions which appeared at average water loadings between 1.6 and 9.1 equiv H_2O/BAS, though the protonation state of the microscopic 2-water cluster was not assigned.[23]

Time-resolved vibrational spectroscopy can access additional experimental information about the structure and dynamics of water and protons in zeolite. Picosecond transient absorption studies demonstrated that vibrational energy is rapidly redistributed from the high-frequency BAS O−H stretch to lower-frequency framework vibrations.[41,42] More recently, experimental capabilities have been extended to ultrafast two-dimensional IR (2D IR) studies of zeolites and other porous materials.[43−45] Among other advantages, 2D IR spectroscopy resolves spectral information as a function of both excitation and detection frequencies, enabling both selective excitation and enhanced resolution for interpreting congested spectra.

In this work, we report linear absorption and 2D IR spectra of hydrated HZSM-5 zeolite at a constant temperature over the range of 1−8 equiv H_2O. This builds on our previous study of high-hydration HZSM-5,[43] extending the hydration range and spectral region probed by 2D IR spectroscopy. The 2D IR spectra, particularly at 1 equiv H_2O, display peculiar features which cast doubt on the most common interpretation of the linear IR spectrum.[37,38] Samples were prepared with an *ex situ* hydration methodology which enabled quantitative control over the hydration level at a constant temperature. Analysis of this data identified distinct signatures of protonated BAS and protonated water cluster, showing experimental evidence that the BAS is deprotonated in the presence of two or more water molecules. From this analysis, we report measured values for the heat of adsorption for the first two water molecules and a deprotonation energy of 1.6 kcal/mol. In the case of the adsorbed water dimer, we see no evidence of a stable protonated zeolite state, which is often predicted by simulations.

These results form a quantitative experimental benchmark for comparison to simulations as a function of water loading. We also report *ab initio* molecular dynamics (AIMD) simulations on clusters of 1−8 H_2O molecules confined in HZSM-5 which display both protonation behavior and calculated spectral trends consistent with our experiments. To further investigate the water structure around the proton, we applied the recently developed rCEC method[46,47] to quantify the location and delocalization of the proton charge defect. This analysis revealed that the excess charge is located preferentially near the most highly coordinated water molecules and remains relatively localized between two oxygen atoms even in the largest clusters.

2. METHODS

2.1. Sample Preparation. A full description of the sample preparation has been reported previously,[43] and additional details are in the Supporting Information (SI). Briefly, HZSM-5(17) zeolites (received from Johnson Matthey) were calcined in air, dehydrated on a Schlenk line with vacuum, and then rehydrated at 150 °C to a fixed level in a sealed Parr acid digestion chamber. The hydration level was measured by titration with methanol. Hydrated zeolites were suspended in a mixture of oils (Flurolube polychlorotrifluoroethylene and perfluoro(tetradecahydrophenanthrene)) which prevented exchange of water with the atmosphere. The Si:Al ratio was 17:1 for all samples, as measured by inductively coupled plasma−optical emission spectroscopy (ICP-OES).

2.2. IR Spectroscopy. IR spectra were collected with samples suspended between two 1 mm CaF_2 windows. Spectral decomposition used maximum entropy reweighting of SVD components based on the method of Widjaja and Garland.[69] 2D IR and transient absorption spectra were collected with polarization control using a spectrometer that has been described previously.[70,71] Scatter artifacts were suppressed with a combination of chopping both pump and probe beams, quasi-phase cycling[72] by oscillating the probe delay stage, and negative time subtraction, as described previously.[43] Additional details describing data collection and analysis can be found in the Supporting Information.

2.3. AIMD Simulations. The atomistic modeling of the protonated water cluster includes a BAS residing in a two-unit cell ZSM-5 zeolite framework (l_a = 20.090 Å, l_b = 19.736 Å, l_c = 26.284 Å),[73] an excess proton to balance the negative charge at the Aluminum T11 site, and a water molecular cluster $(H_2O)_n$ consisted of 1, 2, 3, 4, 6, or 8 water molecules near the BAS. To capture proton shuttling within the cluster and at the interface, as well as the dynamics and statistical distributions of the protonated water cluster at each hydration level, the zeolite framework and the protonated water cluster were treated explicitly with quantum mechanical calculations at the DFT/revPBE/DZVP (revPBE-D3) level of theory.[74] The CP2K package[75] was used to carry out the AIMD simulation using the Quickstep code[76] and the hybrid Gaussian and plane waves (GPW) method[77] with the Goedecker−Teter−Hutter pseudopotential parameterized for the PBE functional.[78] Grimme's D3 dispersion correction was applied to the long-range interactions using a cutoff distance of 40 Å.[79] All AIMD simulations of protonated water clusters are integrated with an MD time step of 0.5 fs at 298 K to sample configurations in the constant NVT ensemble with a Nose−Hoover thermostat and a time constant of 1 ps. For each protonated cluster, the AIMD simulation was first equilibrated for ∼4 ps prior to a production run of ∼20 ps.

The power spectra of protonated water clusters were calculated from Fourier transform of the velocity autocorrelation function of each H atom. Since the protonic excess charge is delocalized in the hydrogen-bond network, it is described by the CEC position rather than a localized atomic position. The rCEC approach[46,47] was used to assign the CEC positions in the AIMD trajectories of protonated water clusters at BAS. The rCEC analysis also provides the distribution of the excess charge in the BAS oxygen atoms and all water molecules. Further details of the AIMD methodology were reported previously,[43] and the rCEC analysis is elaborated in the Supporting Information.

3. RESULTS AND DISCUSSION

3.1. Controlled Hydration of Zeolites. Sample preparation was a crucial component for hydration-dependent IR spectroscopy, which required quantitative control of the adsorbed water per acid site. The methodology was based on previously published work[43] and is detailed in the SI. Here, we

https://doi.org/10.1021/acs.jpcc.3c03611
J. Phys. Chem. C 2023, 127, 16175−16186

extend that methodology to a much wider hydration range than in our previous study. HZSM-5 samples were hydrated *ex situ* by equilibration with water vapor, then suspended in a mixture of hydrophobic index-matching oils for spectroscopic experiments. The mean hydration level of each sample, $\bar{h}$, is the ratio of adsorbed water to Al content, measured by methanol titration and ICP-OES, respectively. As a simple ratio between two directly measured quantities, this measurement of the hydration level does not require calibration to a second experiment such as thermogravimetric analysis or isothermal adsorption, which is a drawback of the more common *in situ* method. For measuring 2D IR spectra of water in zeolites, the greatest challenge is the significant scattered light from micron-size particles.[43,44] The *ex situ* hydration method enables suspension in index-matching oils, which significantly reduces scatter in nonlinear IR spectroscopy.[43,45] A Si/Al ratio of 17:1 was used to reach a sufficient signal/scatter ratio in nonlinear experiments.

3.2. Hydration-Dependent Infrared Spectroscopy and Spectral Decomposition. FTIR spectra of H_2O in HZSM-5(17) zeolites were measured as a function of hydration level from 0.5 to 8.0 equiv H_2O per Al (Figure 1).

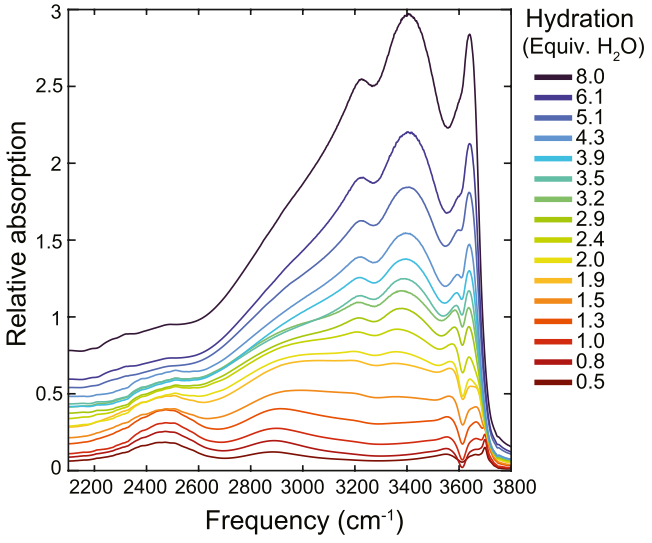

Figure 1. FTIR hydration series. FTIR spectra of HZSM-5 from 0.5 to 8.0 equiv H_2O/Al. Spectra were normalized to the water stretch-bend combination band at 5260 cm^{-1} (Figure S5) and scaled to the measured hydration level, then the dehydrated zeolite spectrum was subtracted.

In Figure 1, the dehydrated zeolite spectrum was subtracted; the series without subtraction is shown in Figure S5. At low hydration, 0.5−1.0 equiv H_2O, the most prominent spectroscopic feature is a broad doublet peaked near 2500 and 2850 cm^{-1}. The depletion at 3610 cm^{-1} arises from the subtraction of the O−H stretch of dehydrated BAS, and adsorbed water-free O−H appears at 3700 cm^{-1}. The doublet is often assigned to Fermi resonance between red-shifted zeolitic bridging O−H stretch and O−H−O bend overtone.[16,21,22,37−39] While the character of the band can be debated, it is unambiguous that the doublet arises from the H-bonded zeolite BAS O−H stretch, as the same feature appears for a range of H-bond acceptors including molecules such as dimethyl ether and THF, which lack intramolecular O−H bonds.[16,37] Therefore, in the hydrated zeolite system, this feature is a signature of protonated zeolite BAS donating a H-bond to adsorbed H_2O.

The IR spectrum changes markedly with increasing hydration, gaining intensity across the O−H stretch frequency range. At high hydration, 4−8 equiv H_2O, a prominent set of features arise centered at high frequencies, with a broad tail extending across the observed spectral region. On the basis of 2D IR spectroscopy, AIMD simulations, and spectral calculations, we recently assigned the features at 3220, 3400, and 3640 cm^{-1} to the water stretch-bend Fermi resonance (FR), H-bonded O−H stretch, and free O−H stretch, respectively.[43] We assigned the broad continuum absorption as a signature of the hydrated proton, as a qualitatively similar feature is observed in the liquid[48,49] and protonated gas-phase water clusters.[50] At lower frequencies, below 2100 cm^{-1}, water and proton features are distorted by zeolite framework vibrations (Figure S5).

While variations in the IR spectrum represent changes in the populations of water molecules in different environments and protonation states, a quantitative analysis is complicated by the broad and overlapping spectral signatures. Furthermore, due to non-Condon effects in vibrational O−H stretch spectroscopy,[51] the absorption cross section is expected to vary for water molecules in different environments.

We sought a quantitative relationship between changes in the IR spectrum and populations of water molecules in specific environments with distinct spectral signatures $S_n(\omega)$ and the hydration-dependent populations in those environments $C_n(\bar{h})$. To deconvolve the overlapping features, we expressed the hydration series absorbance $A(\bar{h},\omega)$ as a linear combination of three components labeled α, β, and γ.

$$A(\bar{h}, \omega) = \sum_{n=\alpha,\beta,\gamma} C_n(\bar{h})\varepsilon_n S_n(\omega) \tag{1}$$

Component spectra and amplitudes were computed using singular value decomposition (SVD) with reweighted components subject to maximum entropy, positivity, and dissimilarity constraints (details in the SI). The resulting area-normalized component spectra are displayed in Figure 2a.

To account for differences in absorption cross sections between spectral components, the component populations were constrained to sum to the hydration level.

$$\bar{h} = \sum_{n} C_n(\bar{h}) \tag{2}$$

The relative absorption cross sections—integrated over the frequency axis—are contained in the fitted values ε_n, yielding $\varepsilon_\beta/\varepsilon_\gamma = 2.6$ and $\varepsilon_\alpha/\varepsilon_\gamma = 0.96$. The hydration-dependent amplitude $C_n(\bar{h})$ of component n is proportional to the population of water molecules with spectrum $S_n(\omega)$ at mean hydration level $\bar{h}$, shown in Figure 2b. Figure 2c shows the populations of the three components as fractions of the total water adsorbed, $C_n/\bar{h}$.

Next, we assigned the components to their respective molecular environments using their spectral signatures. S_α strongly resembles the spectrum at low hydration, capturing the broad doublet, water-free O−H stretch, and subtraction of the dry zeolite bridging O−H stretch. Therefore, we assigned component α to the protonated BAS donating a H-bond to adsorbed water. S_γ strongly resembles the spectrum at high hydration, capturing the prominent water stretch-bend FR, water−water H-bond, and free O−H features. Therefore, we

https://doi.org/10.1021/acs.jpcc.3c03611
J. Phys. Chem. C 2023, 127, 16175−16186

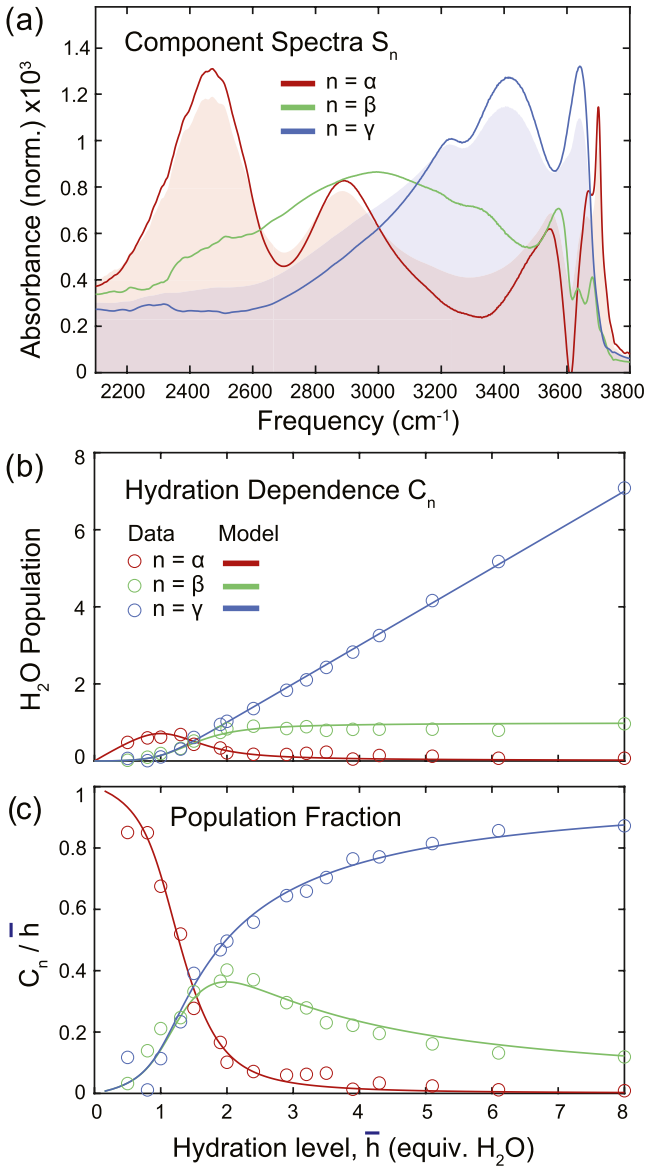

Figure 2. Spectral decomposition using constrained SVD analysis. (a) Area-normalized spectral components with hydration dependence presented as (b) distribution of all H_2O molecules among α, β, and γ environments and (c) the corresponding population fractions. The components report on water and protons in different environments. Components α and β report on the protonation state, with component α representing protonated zeolite BAS donating a H-bond and component β representing excess proton. Component γ is the signature of additional water molecules that are not strongly perturbed by the excess proton. Shaded curves in (a) are area-normalized spectra at 0.5 equiv (red) and 8.0 equiv (blue). Solid lines in (b) and (c) are the fit to a modified BET model described in the text.

assigned component γ to the addition of water molecules to a water cluster. Comparing S_γ to the high-hydration spectrum, intensity is missing in the broad low-frequency shoulder, which we previously assigned to the excess proton.[43] This broad feature is captured by S_β, which spans nearly the entire spectral range in Figure 1.

The hydration-dependent populations of the components (Figure 2b,c) are consistent with these assignments. At low hydration, C_α accounts for the majority of the adsorbed water molecules, but it falls off steeply accounting for only 10% of the population by 2 equiv H_2O. This is the expected behavior of a protonated zeolite component since the BAS becomes deprotonated at higher hydration.[21,23,25] C_β rises steeply from 0.5 to 2.0 equiv H_2O, then plateaus at higher hydration. This is the expected behavior of an excess proton component, which grows as the zeolite is deprotonated and reaches a constant value once deprotonation is complete. C_γ grows slowly at low hydration, then linearly with hydration above 2.0 equiv H_2O, consistent with a component capturing the addition of water not strongly influenced by the excess proton.

Therefore, the spectral decomposition allows us to extract quantitative trends describing the changes in protonation state and water environments as a function of hydration level. However, the linear decomposition is a simplifying assumption that does not account for changes in the individual component spectra with hydration. This could be an issue if the excess proton spectrum varies dramatically between clusters of 2−8 H_2O, as is the case in cold gas-phase protonated water clusters.[50] Figure S7 shows that the reconstruction with three components has excellent agreement with the measurement, with coefficient of determination $R^2 > 0.99$ and without large systematic errors indicative of spectral shifts. Most likely the excess proton spectrum varies somewhat with cluster size, but the linewidth of the feature is so broad at room temperature that those shifts are relatively small and can be neglected to a good approximation.

3.3. 2D IR Spectroscopy with Variable Hydration. To further validate the spectral decomposition, we investigated the persistence of the doublet feature S_α by measuring 2D IR spectra as a function of hydration. 2D IR spectroscopy can more selectively probe this feature, without the use of spectral decomposition, by exciting the lower-frequency band at 2500 cm^{-1} where spectral overlap with other features is minimized. Therefore, the hydration trend of this 2D IR feature can be used to test the hydration trend in component α from the spectral decomposition result.

Figure 3 shows the 2D IR hydration series with excitation centered at 2500 cm^{-1}, measured at 100 fs waiting time. At 1 equiv H_2O, a diagonal feature at 2500 cm^{-1} is observed alongside a prominent cross-peak to the higher-frequency band of the doublet at 2850 cm^{-1}. This is the 2D IR signature of the doublet corresponding to protonated zeolite BAS donating a H-bond. The lineshape displays homogeneous broadening, with equal diagonal and antidiagonal linewidths of 170 cm^{-1} FWHM in the isotropic spectrum (Figure S13). The transient absorption spectrum (Figure S14) shows the feature is short-lived with a population relaxation timescale of ≤190 fs. Using that timescale, we estimate a lifetime broadening of ∼175 cm^{-1}, which accounts entirely for the 2D IR linewidth. The fast population relaxation is consistent with previous suggestions that the zeolitic H-bonded O−H stretch is coupled to O−O stretching[16,38] and other low-frequency modes, providing a route for rapid nonradiative relaxation.

The predominant signature of a homogeneously rounded diagonal and cross-peak is clearly observed from 1 to 2 equiv H_2O and appears to be present up to 4 equiv, although now overlapped with the growing excess proton continuum. By 8 equiv H_2O, the predominant signature in the 2D IR spectrum no longer resembles the low-hydration doublet, instead displaying a more intense excited-state absorption below ω_{Det} = 2400 cm^{-1}.

The 2D IR spectrum of the low hydration doublet is highly unusual due to the lack of clear, high-intensity induced

https://doi.org/10.1021/acs.jpcc.3c03611
J. Phys. Chem. C 2023, 127, 16175−16186

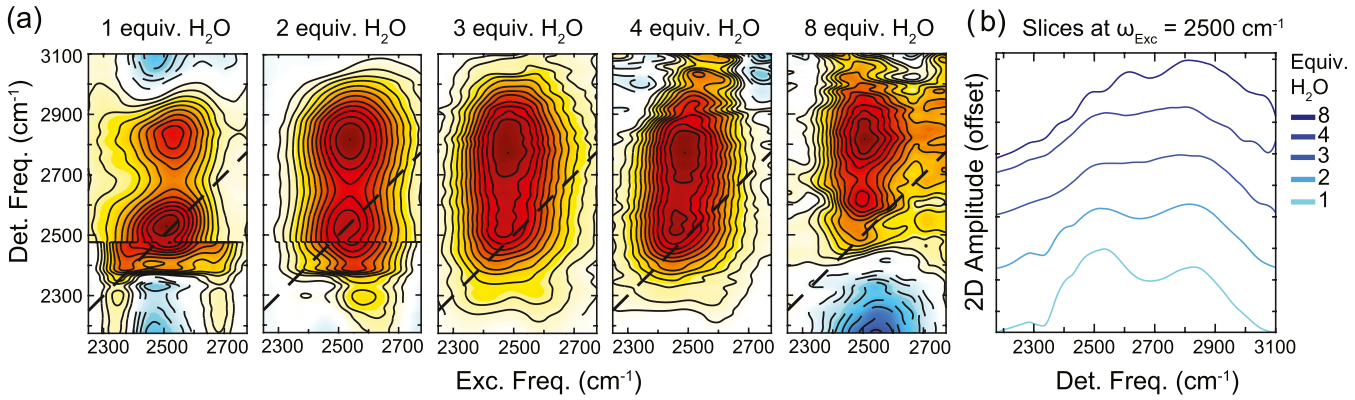

Figure 3. 2D IR hydration series. (a) 2D IR hydration series of HZSM-5 at 100 fs waiting time and perpendicular polarization, excited with pulses centered at 2500 cm^{-1}. (b) Slices of the spectra at excitation frequency 2500 cm^{-1}. The relative intensities of major features do not have a strong polarization dependence, as shown in Figure S12; perpendicular (ZZYY) spectra are displayed to minimize scatter artifacts.

absorption resonances. While the assignment of the doublet to the protonated BAS donating a H-bond to water is firmly rooted in experimental evidence,[16,52] the 2D IR spectrum provides further information about the nature of the vibrations giving rise to the bands. The traditional explanation for the splitting has been stretch-bend Fermi resonance,[37−40] though that assignment does not explain the missing induced absorption intensity in the 2D IR spectrum.[53] In fact, model 2D IR spectra based on Fermi resonance coupling predict an intense induced absorption at an intermediate detection frequency between the two prominent features in Figure 3a, which is clearly not observed.[53] Further 2D IR experiments and analysis may reveal anharmonic couplings or higher-lying vibrational states, which can provide additional constraints on this problem. For now, we treat the doublet merely as a fingerprint of the protonated BAS state.

3.4. Modified BET Model for Hydration Dependence.

The spectra in Figures 1−3 are ensemble measurements at macroscopic hydration level $\overline{h}$, which is an average over the distribution of microscopic hydration numbers h = 0,1,2⋯ Therefore, there are two possible explanations for the presence of the protonated BAS signature α at $\overline{h}$ = 2: (a) both protonated BAS and excess proton are stable species in adsorbed water dimer clusters or (b) protonated BAS is only stable in the adsorbed water monomer, but there is a substantial fraction of clusters with h = 1 at mean hydration level $\overline{h}$ = 2. To distinguish between these possibilities, a model is needed which can relate the mean water adsorbed per site $\overline{h}$ to the distribution of adsorbed cluster sizes $\{\theta_h\}$, where θ_h is the fraction of sites occupied by clusters of size h.

To do so, we considered the preparation of the hydrated samples, where zeolites were equilibrated with water vapor in a sealed container at 150 °C. We modeled this equilibrium using a modified Brunauer−Emmett−Teller (BET) theory[54] described in the SI. In this model, equilibrium is reached between water adsorbed on the zeolite sites and water in the gas phase at partial pressure P_{H_2O} according to a system of equations for sequential adsorption events.

$$\theta_h + H_2O \rightleftharpoons \theta_{h+1},\ K_{h+1} \tag{3}$$

The adsorbed first and second water molecules at the BAS are treated with distinct equilibrium constants K_1 and K_2, and all subsequent steps are described by $K_L = 1/P_0$, the equilibrium constant for liquefaction. P_0 is the saturation partial pressure, and equilibrium constants are related to heats of adsorption q_h by $K_h = \exp(q_h/k_BT)$. This treatment of K_h for subsequent adsorption steps is a reasonable approximation, based on adsorption studies showing that the heat of adsorption decreases with hydration and varies gradually at hydration levels greater than 2.[55−57] The system of equations, eq 3, was solved to relate the fractional coverages θ_h to the partial pressure $x = P_{H_2O}/P_0$, the amount of water adsorbed in clusters of size h, $N_h = h\theta_h$, and the average water cluster size $\overline{h} = \sum_h h\theta_h$. By treating x as an implicit variable, we expressed θ_h as a function of $\overline{h}$, subject to two parameters $b_1 = K_1/K_L$ and $b_2 = K_2/K_L$ (see SI).

Finally, the derived expressions for the distribution of adsorbed molecules in clusters of size h were related to the populations, or number of molecules, displaying spectral signatures α, β, and γ (representing protonated BAS, excess proton, and additional adsorbed water molecules, respectively). We assume that S_α arises only from singly hydrated sites; therefore, C_α is given by the fraction of sites with h = 1.

$$C_\alpha = \theta_1 \tag{4}$$

Since a hydrated site can either be protonated with signature S_α or deprotonated with signature S_β, C_β is the fraction of sites hydrated by two or more molecules.

$$C_\beta = \sum_{h\geq 2} \theta_h \tag{5}$$

Then, in clusters of size two or more, one water molecule is accounted for by C_β and the rest are accounted for by C_γ. The number of subsequent water molecules is given by the total molecules adsorbed in clusters of two or more, subtracting the first molecule in those clusters.

$$C_\gamma = \sum_{h\geq 2} (h-1)\theta_h \tag{6}$$

Equations 4−6 comprise a model of $C_n(\overline{h})$ with fit parameters b_1 and b_2. Fitting that model to the data yielded b_1 = 180 and b_2 = 7 with the resulting curves plotted in Figure 2b,c and coefficient of determination $R^2 > 0.99$. Using the preparation temperature of 150 °C, this corresponds to the relative heats of adsorption for the first two water molecules $\Delta q_1 = q_1 - q_L$ = 4.4 kcal/mol and Δq_2 = 1.6 kcal/mol. Using the heat of liquefaction[58] q_L = 9.1 kcal/mol at 150 °C results in q_1 = 13.5 kcal/mol and q_2 = 10.7 kcal/mol, both falling within the range of previous measurements.[35,55−57]

https://doi.org/10.1021/acs.jpcc.3c03611
J. Phys. Chem. C 2023, 127, 16175−16186

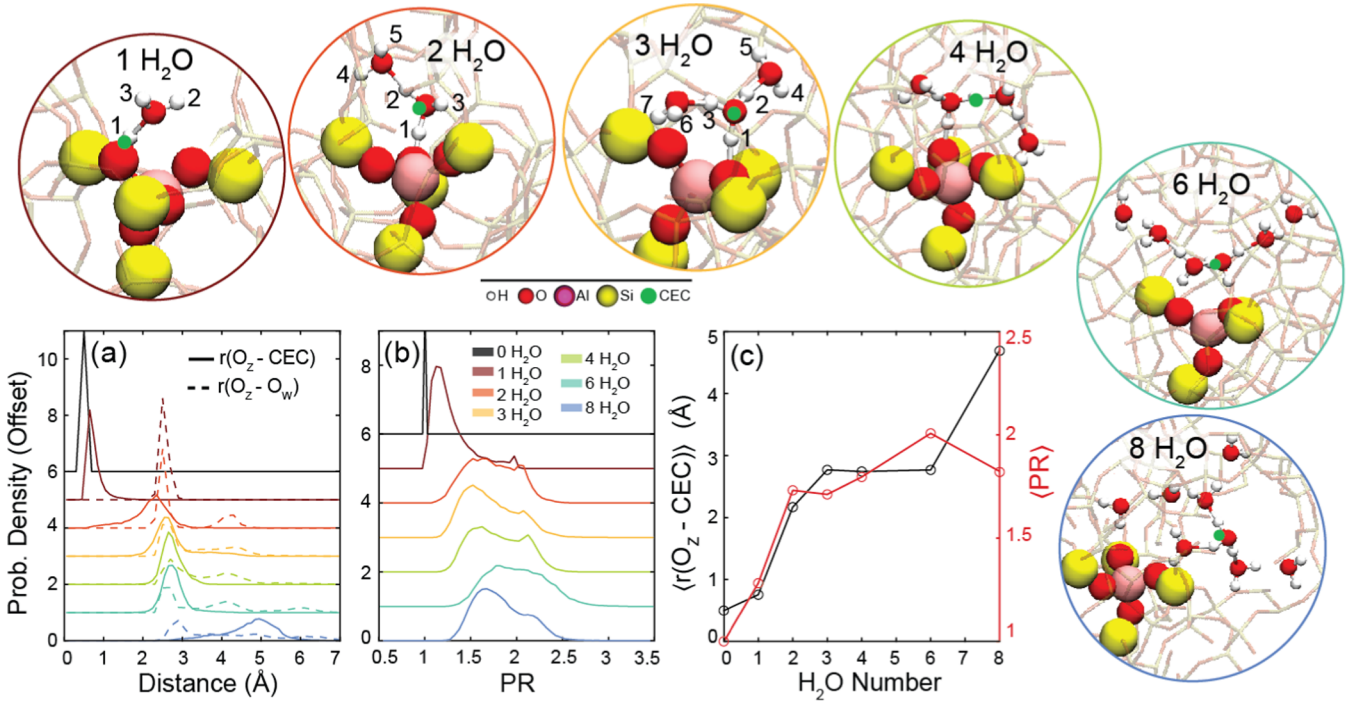

Figure 4. AIMD trajectory statistics of CEC position and delocalization. (a) Distribution of distances between the zeolite oxygen atom (O_Z) and center of excess charge (CEC, solid lines), overlaid with the distribution of water oxygen (O_W) atoms (dashed lines). (b) Proton charge delocalization, represented by the distribution of participation ratios (PR).[63,64] Probability distributions are offset by 1 unit for clarity. (c) Expectation values of r(O_Z-CEC) and PR as a function of water cluster size. Representative trajectory snapshots from AIMD simulations of 1−8 H_2O molecules in HZSM-5 are displayed above and labeled by the number of H_2O molecules. The CEC, which represents the excess proton charge location, is displayed in each configuration as a green dot. Hydrogen atoms in snapshots of 1−3 H_2O molecules are numbered for reference.

Setting $b_2 = 1$ returns the model to the typical BET theory, where only the first adsorption has a distinct equilibrium constant. Under that assumption, the data was reasonably well fit except for the region near $\bar{h} = 2$, where the model then underestimated C_β (Figure S11). Increasing $b_2 > 1$ accounts for an additional stabilization energy upon adsorption of the second water molecule. That energy can be attributed to the stabilization associated with proton dissociation which we estimate as $\Delta q_2 = 1.6$ kcal/mol. This measured value can provide a benchmark for evaluating the accuracy of theoretical methods for simulating deprotonation in zeolites, where the choice of density functional can have a large effect on the protonation behavior.[32]

This analysis shows that the hydration-dependent IR spectra of HZSM-5 can be captured quantitatively by a model which treats the proton as dissociated from the BAS when 2 or more molecules are adsorbed; the presence of a stable protonated BAS state in adsorbed water dimers is not necessary. In this framework, the persistence of the signature C_α until ∼4 equiv H_2O is accounted for by the distribution of microscopic hydration environments, which includes a fraction of singly hydrated sites at higher hydration levels.

3.5. AIMD Simulation of 1−8 H_2O Molecules at the Brønsted Acid Site. To understand the spectroscopic components at atomistic detail—particularly the trends near 2 equiv H_2O—and to further investigate the evolution of the protonation state as a function of adsorbed water cluster size, AIMD simulations were performed at the revPBE-D3 level of theory with 0−8 H_2O molecules equilibrated in HZSM-5 at 298 K. The revPBE-D3 functional has been shown to have good performance for water, including at the interface of acidic zeolite.[32,S9−62] Seven independent trajectories were analyzed, revealing connections between calculated atomic positions, charge location and delocalization, and vibrational spectra.

The H-bond network is relatively simple at lower hydration numbers (1−3 H_2O) and becomes complicated with increasing cluster size. Beyond 2 H_2O molecules, numerous potential energy minimum structures can be located through geometry optimization at 0 K, but only a few are statistically meaningful at room temperature. The most representative configurations of adsorbed water clusters at the BAS are shown in Figure 4.

H-bond formation was observed between water molecules and one or more oxygen atoms in the BAS (the 4 nearest-neighbor oxygens to Al), which we will refer to as interfacial H-bonds. H-bonding was not observed in any other framework oxygen atoms. At an equilibrated state, the hydrogen-bond configuration within the protonated water cluster was relatively stable, and at least one interfacial H-bond remained intact during each simulation. When two or more interfacial H-bonds were present, the bond with the shortest O−O distance was identified and the participating zeolite and water oxygens were labeled O_Z and O_{W1}.

The distributions of O_Z−O_W distances are displayed as dashed lines in Figure 4a. The most probable distance from O_Z to the first water oxygen is 2.5 Å when one water is present and increases with cluster size to 2.9 Å in the 8-water cluster. The second and third adsorbed water molecules form H-bonds to the first with O_Z−O_W distances of ∼4 Å. In larger clusters, the constrained geometry of the zeolite channels influences the H-bonding network, causing some branching into the pores and not necessarily maximizing water−water H-bonds. For example, in the representative snapshot for 6 H_2O the only triply coordinated water molecules are coordinated to a zeolite

https://doi.org/10.1021/acs.jpcc.3c03611
J. Phys. Chem. C 2023, 127, 16175−16186

oxygen, while the 8-water cluster supports triple-coordination to three other water molecules.

The charge distribution associated with the excess proton and its hydration dependence was quantified using the rCEC approach adopted from Li et al.[46,47] Based on the multistate empirical valence bond (MS-EVB) method developed by the Voth group,[65−67] r^{CEC} is a collective variable which describes the location of the center of excess charge (CEC) associated with the net positive charge defect from the excess proton. In this method, the adiabatic ground state of a configuration as a function of the nuclear coordinates is expressed on a basis of diabatic states determined by the H-bonding topology.

$$|\psi^{adi}\rangle = \sum_i c_i |\psi_i^{dia}\rangle \tag{7}$$

Each diabatic state represents a localized excess charge near a single oxygen atom, defined by its center-of-charge (COC) position $\mathbf{r}^{COC}$. For a molecular cluster with h H_2O molecules at the BAS, there are $h + 4$ basis states, one for each H_2O oxygen atom plus the four zeolitic oxygen atoms bonded to Al. The squared expansion coefficient c_i^2 represents the distribution of proton excess charge in the ith diabatic state. In the rCEC method, the weights of adjacent diabatic states are parameterized based on the interatomic O−H−O distances using constrained DFT calculations.[68] The CEC position $\mathbf{r}^{CEC}$ is then the weighted average of the COC positions.

$$\mathbf{r}^{CEC} = \sum_i c_i^2 \mathbf{r}_i^{COC} \tag{8}$$

Trajectory statistics of the CEC position with respect to O_Z, $r(O_Z{-}CEC)$, are displayed in Figure 4a next to the $r(O_Z{-}O_W)$ distributions. The distribution of $r(O_Z{-}CEC)$ increases modestly with the addition of the first water molecule, then increases more dramatically with the addition of the second. From 2 to 4 H_2O molecules, the center of the $r(O_Z{-}CEC)$ distribution displays a much smaller positive shift, while the tails have different behavior. The distribution for 2 H_2O has a tail to smaller distances, indicating charge sharing between O_{W1} and O_Z. While there is little change in the CEC position from 3 to 6 H_2O, there is an increase of about 2 Å from 6 to 8 H_2O.

In the 8 H_2O cluster, the proton charge is statistically located near the periphery of the cluster, shared between water molecules that are not coordinated to a zeolitic oxygen. This shifting of the excess proton position away from the deprotonated BAS at high hydration numbers was also captured in metadynamics simulations by Grifoni et al.[25] This observation could be neither verified nor disputed on the basis of FTIR spectroscopy experiments, as we did not resolve any changes in the measured excess proton IR spectrum from 6 to 8 equiv H_2O. Spectral calculations based on the CEC time correlation function also displayed little change from 6 to 8 H_2O, suggesting that the proton spectrum is relatively insensitive to the exact position in the cluster once the BAS is deprotonated (Figure S24).

The delocalization of the proton charge defect was quantified using the participation ratio (PR) at each hydration number. The PR, shown in Figure 4b, is a measure of the number of diabatic states that contribute effectively to the state of the excess proton.[63,64]

$$PR = \left(\sum_i c_i^4\right)^{-1} \tag{9}$$

The PR ranges from PR = 1 for a localized state to N for full delocalization over N basis states. In the absence of water, the excess charge is localized on a single O_Z and the PR distribution is a delta function at unity. When water is present, the PR distribution displays a large shift from 1 H_2O to 2 H_2O and relatively minor changes at higher hydration. At 1 H_2O, the excess charge is largely localized in a single state (mean value PR = 1.2 corresponds to approximately $c_1^2 = 0.9$ and $c_2^2 = 0.1$), with a tail to larger values indicating a small fraction of configurations where there is increased charge sharing with the adsorbed H_2O molecule. For 2−8 H_2O, the PR assumes a roughly bimodal distribution peaked near PR = 1.5 & 2. This indicates that the protonic charge is largely shared unequally between two states. Interestingly, while the number of diabatic states grows linearly with the number of water molecules, the PR does not. The PR never approaches a value of 3, indicating that most of the protonic charge remains relatively localized along a single O−H−O axis. Notably, an assignment of partial atomic charges (Figure S25) supports the conclusions of the rCEC analysis.

3.6. Hydrogen Atomic Positions. In addition to the charge distribution, the protonation state is related to the atomic positions of hydrogen atoms. To investigate the proton dissociation from BAS to water cluster, we consider the statistics of hydrogen atom locations along selected O−H−O axes for 1−3 H_2O molecules. Trajectory statistics were used to calculate the potential of mean force (PMF) between O_Z and the adsorbed water oxygen O_{W1} as a function of $\delta r(O_Z{-}H{-}O_{W1}) = r(O_Z{-}H) - r(O_{W1}{-}H)$, shown in Figure 5a. The PMF minimum shifts from $\delta r = -0.5$ Å at 1 H_2O to +0.3 Å at 2 H_2O and +0.5 Å at 3 H_2O, showing that the most probable proton position switches from the O_Z side of the axis to the O_{W1} side between 1 and 2 H_2O, and moves even closer to O_{W1} at 3 H_2O.

Proton sharing between water molecules is visualized by the PMF along the $O_{W1}{-}H{-}O_{W2}$ axis (Figure 5b), where O_{W2} is defined as the water oxygen closest to O_{W1} at a given trajectory snapshot. When 2 H_2O molecules are present, the PMF across the $O_{W1}{-}H{-}O_{W2}$ axis favors O_{W1} with a minimum at $\delta r = -0.5$ Å. At 3 H_2O, the PMF retains that global minimum and gains an additional local minimum at $\delta r = +0.3$ Å. The shape of this PMF is a result of water trimer configurations such as the one pictured in Figure 4 where the first H_2O molecule is H-bonded to two other water molecules, and thus has two potential partners for proton sharing. When the excess proton is not shared with O_{W2}, then the hydrogen atom along that axis is bound to O_{W1} with PMF minimum at $\delta r = -0.5$ Å, while states with asymmetric proton sharing between O_{W1} and O_{W2} account for the additional local minimum at $\delta r = +0.3$ Å. Together, the results in Figure 5 show that atomic hydrogen positions follow a similar trend as the charge distribution, consistent with the assignment of a shared proton in clusters of 2−3 H_2O molecules and proton sharing between O_Z and O_W in the adsorbed dimer.

3.7. Spectral Analysis. To draw connections between hydration, molecular structure, and vibrational spectra, both harmonic normal modes and anharmonic power spectra were calculated. Harmonic spectra of optimized clusters are displayed in Figures S15−S17. While O−H stretch normal

https://doi.org/10.1021/acs.jpcc.3c03611
J. Phys. Chem. C 2023, 127, 16175−16186

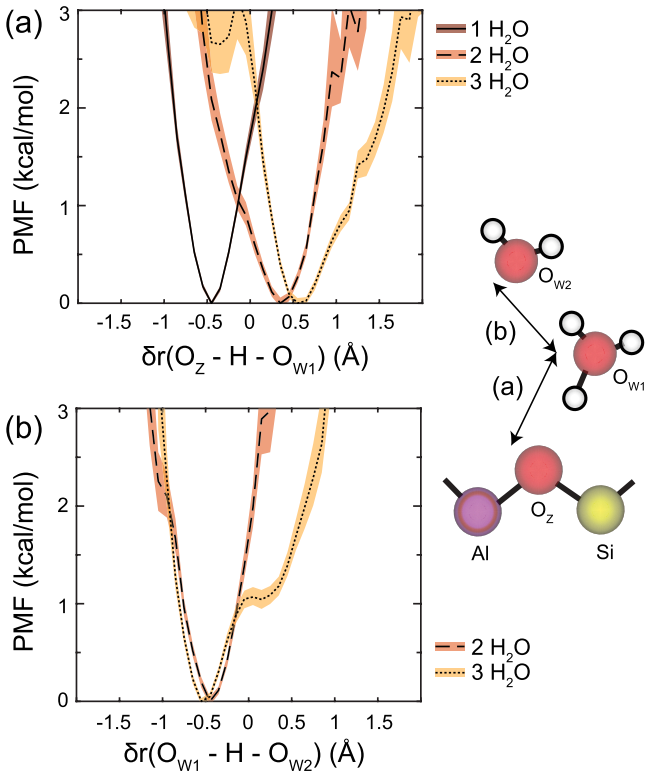

Figure 5. Potential of mean force (PMF) at 298 K. (a) O_Z−H−O_{W1} axis between the zeolite oxygen and nearest water oxygen and (b) the O_{W1}−H−O_{W2} axis between the first two water oxygen atoms. The hydrogen atom position is described by the difference between O−H distances, $\delta r(O_A–H–O_B) = r(O_A–H) - r(O_B–H)$. Shaded curves denote error bars calculated with the bootstrap method. The cartoon on the right depicts an adsorbed water dimer labeling the O−H−O axes considered in (a, b).

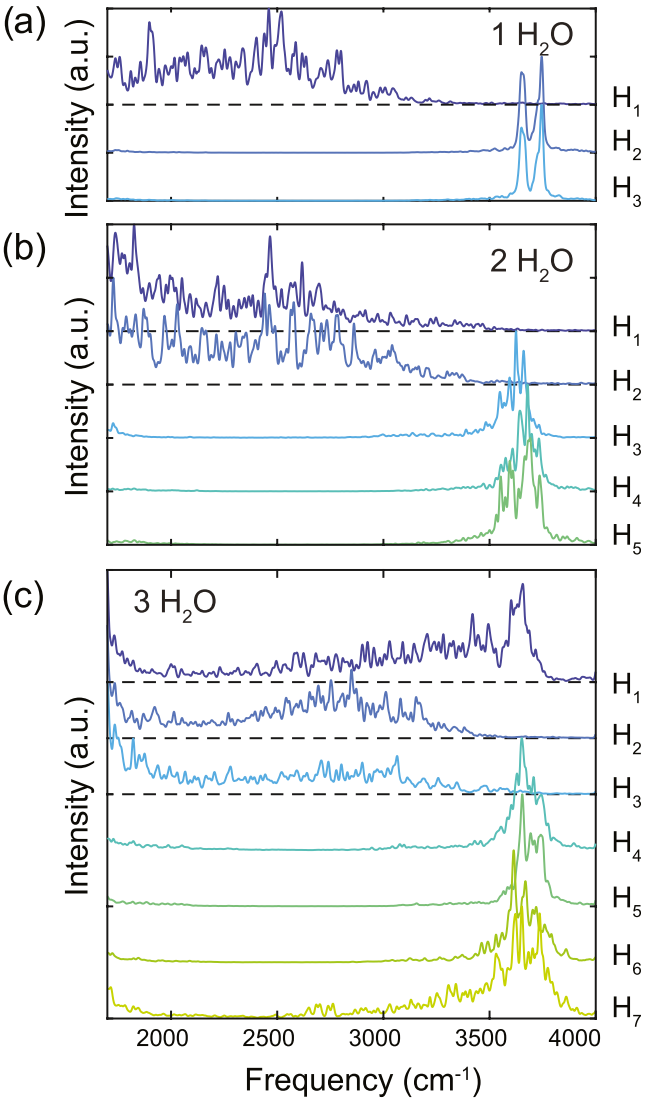

Figure 6. Power spectra of individual hydrogen atoms. Optimized clusters of (a) 1 H_2O, (b) 2 H_2O, and (c) 3 H_2O are shown. Hydrogen atoms are labeled by number, corresponding to the labels in Figure 4. Spectra are offset for clarity; dashed lines are baselines.

modes fall broadly in the expected frequency ranges, harmonic spectra are limited for describing the highly anharmonic vibrations of water and protons.[49] Instead, we considered power spectra of individual hydrogen atoms in clusters of 1−3 H_2O, which each correspond to the motions of the selected atom. Power spectra are shown in Figure 6 following the hydrogen atom numbering in Figure 4. This approach better reflects the anharmonicity of the vibrations and relates calculated frequencies to molecular environments with atomic specificity.

The power spectra in Figure 6 display either a broad proton feature spanning ca. 2000−3000 cm^{-1} or narrow free O−H features >3500 cm^{-1}. The proton feature is most prominent in the spectra of H_1 (1 H_2O), H_1 & H_2 (2 H_2O), and H_2 & H_3 (3 H_2O). The evolution of that feature correlates well to the movement of the CEC and atomic hydrogen positions in Figures 4−5. The spectra of H_1 & H_7 in the 3 H_2O cluster—both located along a O_W−H−O_Z axis—display some spectral density between ca. 3000 and 3500 cm^{-1}, reflecting interfacial H-bond formation. Broadening of the free O−H features and growth in the H-bonded O−H region with increasing hydration agrees qualitatively with trends in the experimental IR spectrum.

While power spectra show reasonable agreement with the frequencies and linewidths of experimental excess proton and free O−H features, they notably do not capture the broad doublet feature at 1 H_2O. This may be a result of relatively large-amplitude motions of H_1 (1 H_2O) combined with the ~20 ps trajectory length, which is feasible for AIMD simulations. As a result, modulations in the broad H_1 feature are on the order of the noise level, which could be improved with longer simulation time. Therefore, these spectral calculations are useful for identifying hydrogen atoms that carry some protonic charge—leading to broad low-frequency spectra—but not for discriminating between bound and excess proton states.

3.8. Protonation State and H-Bonding Network.

Taken together, the trends in the AIMD simulations agree with the model of hydration-dependent protonation state that was used to capture the experimental IR spectra. The proton can be described as zeolite-bound in the presence of one H_2O molecule and shared excess proton when two or more H_2O molecules are present. The clear transition between these two states can be observed in the CEC position, PR, and PMF minimum between O_Z and O_{W1}, and is consistent with trends in the power spectra of hydrogen atoms.

The AIMD simulations reveal further atomistic details and connections between the protonation state and H-bonding

https://doi.org/10.1021/acs.jpcc.3c03611
J. Phys. Chem. C 2023, 127, 16175−16186

network. The PR distribution between ~1.5 and 2 for clusters of 2−8 water molecules suggests delocalization over 2 oxygen atoms, leading to the language of a shared proton. While the water dimer is described well by this picture, the proton can be shared either between O_Z and O_{W1} or between O_{W1} and O_{W2}, with roughly equal probability. This is distinct from larger clusters, where the proton is more prominently shared between two water molecules, as seen in the shifts in $r(O_Z\text{-CEC})$, PMF, and hydrogen power spectra. This distinction may account for some of the debate over the description of the water dimer.

Furthermore, the simulation results suggest that the location of the excess proton is strongly influenced by the connectivity of the H-bonding network, which extends to the zeolitic oxygen atoms. The trends in H-bond connectivity and CEC location suggest that the proton charge is located preferentially near the most highly coordinated water molecules. For the small clusters present in confined HZSM-5 pores, the largest coordination number is often 3, and a triply coordinated water molecule is an important structural motif for stabilizing the proton. The adsorbed water trimer is the smallest cluster where a water molecule is triply coordinated, and also the smallest cluster where the proton is shared primarily between water molecules and not with O_Z. At higher hydration, the excess proton charge defect position r^{CEC} moves further from the deprotonated BAS only when water molecules triply coordinated to three O_W become available in the water octamer. Therefore, we suggest a simple scheme for identifying the most probable proton location in adsorbed water clusters: (1) in the adsorbed water monomer, the zeolite BAS is protonated; (2) in the adsorbed water dimer the proton is shared either between O_Z and O_{W1} or between O_{W1} and O_{W2}; and (3) at higher hydration, the proton is shared preferentially between the most highly coordinated water molecules.

4. CONCLUSIONS

We have presented experimental IR spectroscopic evidence identifying the crossover point from protonated zeolite BAS to shared proton. Using a spectral decomposition, we extracted quantitative information from the hydration series of HZSM-5 zeolite prepared at controlled hydration levels. At 1 H_2O, the proton is stabilized on the zeolite BAS. From 2 to 8 H_2O, the proton is instead shared between two oxygen atoms, placing the critical water number at 2 H_2O. A series of AIMD simulations with varying H_2O numbers reproduced the experimental trends in the protonation state and IR spectrum. An analysis of excess charge position, atomic potential of mean force, and local mode power spectra further revealed that the excess protonic charge is shared asymmetrically between two oxygen atoms. The case of the water dimer is distinct because significant sharing occurs between water and the deprotonated BAS, while proton sharing in larger clusters occurs primarily between two water molecules. H-bonding connectivity is important for determining protonation state and location, as the excess proton preferentially occupies locations resembling a triply coordinated hydronium ion. Taken together, these experimental and theoretical results provide a consistent description of the protonation state of the HZSM-5 BAS and its evolution across the hydration range of 1−8 H_2O per acid site.

■ ASSOCIATED CONTENT

Supporting Information

The Supporting Information is available free of charge at https://pubs.acs.org/doi/10.1021/acs.jpcc.3c03611.

Detailed methods section, zeolite characterization, spectral calculations, and Löwdin partial charge assignments (PDF)

■ AUTHOR INFORMATION

Corresponding Author

Andrei Tokmakoff − *Department of Chemistry, James Franck Institute, and Institute for Biophysical Dynamics, The University of Chicago, Chicago, Illinois 60637, United States;* orcid.org/0000-0002-2434-8744; Email: tokmakoff@uchicago.edu

Authors

John H. Hack − *Department of Chemistry, James Franck Institute, and Institute for Biophysical Dynamics, The University of Chicago, Chicago, Illinois 60637, United States;* orcid.org/0000-0003-0042-0921

Xinyou Ma − *Department of Chemistry, James Franck Institute, and Institute for Biophysical Dynamics, The University of Chicago, Chicago, Illinois 60637, United States; Chicago Center for Theoretical Chemistry, The University of Chicago, Chicago, Illinois 60637, United States*

Yaxin Chen − *Department of Chemical and Biological Engineering, Northwestern University, Evanston, Illinois 60208−3120, United States*

James P. Dombrowski − *Department of Chemical and Biological Engineering, Northwestern University, Evanston, Illinois 60208−3120, United States*

Nicholas H. C. Lewis − *Department of Chemistry, James Franck Institute, and Institute for Biophysical Dynamics, The University of Chicago, Chicago, Illinois 60637, United States;* orcid.org/0000-0002-2554-0199

Chenghan Li − *Department of Chemistry, James Franck Institute, and Institute for Biophysical Dynamics, The University of Chicago, Chicago, Illinois 60637, United States; Chicago Center for Theoretical Chemistry, The University of Chicago, Chicago, Illinois 60637, United States*

Harold H. Kung − *Department of Chemical and Biological Engineering, Northwestern University, Evanston, Illinois 60208−3120, United States;* orcid.org/0000-0001-9599-0155

Gregory A. Voth − *Department of Chemistry, James Franck Institute, and Institute for Biophysical Dynamics, The University of Chicago, Chicago, Illinois 60637, United States; Chicago Center for Theoretical Chemistry, The University of Chicago, Chicago, Illinois 60637, United States;* orcid.org/0000-0002-3267-6748

Complete contact information is available at: https://pubs.acs.org/10.1021/acs.jpcc.3c03611

Notes

The authors declare no competing financial interest.

■ ACKNOWLEDGMENTS

This work was supported in part by the Advanced Materials for Energy Water Systems (AMEWS) Center, an Energy Frontier Research Center funded by the U.S. Department of Energy, Office of Science, Basic Energy Sciences. J.H.H. and A.T.

acknowledge funding by the Office of Basic Energy Sciences, U.S. Department of Energy (Grant No. DE-SC0014305). X.M. and G.A.V. were supported by the Office of Naval Research through Award N00014-21-1-2157, and they acknowledge the computational resources provided by the University of Chicago Research Computing Center (RCC) and the U.S. Department of Defense High Performance Computing Modernization Program. The authors acknowledge Johnson Matthey PLC for providing the zeolite samples free of charge and Halocarbon LLC for providing the PCTFE oils free of charge.

■ ABBREVIATIONS

2D IR, two-dimensional infrared; AIMD, *ab initio* molecular dynamics; BAS, Brønsted acid site; CEC, center of excess charge; DFT, density functional theory; equiv, equivalents; FR, Fermi resonance; FTIR, Fourier transform infrared; ICP-OES, inductively coupled plasma−optical emission spectroscopy; MS-EVB, multistate empirical valence bond; PMF, potential of mean force; PR, participation ratio; SVD, singular value decomposition

■ REFERENCES

(1) Davis, M. E. Zeolite-Based Catalysts for Chemicals Synthesis. *Microporous Mesoporous Mater.* **1998**, *21*, 173−182.
(2) Tanabe, K.; Hölderich, W. F. Industrial Application of Solid Acid-Base Catalysts. *Appl. Catal., A* **1999**, *181*, 399−434.
(3) Corma, A. State of the Art and Future Challenges of Zeolites as Catalysts. *J. Catal.* **2003**, *216*, 298−312.
(4) Martínez, C.; Corma, A. Inorganic Molecular Sieves: Preparation, Modification and Industrial Application in Catalytic Processes. *Coord. Chem. Rev.* **2011**, *255*, 1558−1580.
(5) IPCC; 2022. *Climate Change 2022: Mitigation of Climate Change. Contribution of Working Group III to the Sixth Assessment Report of the Intergovernmental Panel on Climate Change*; Shukla, P. R.; Skea, J.; Slade, R.; Al Khourdajie, A.; Diemen, R. van.; McCollum, D.; Pathak, M.; Some, S.; Vyas, P.; Fradera, R.; Belkacemi, M.; Hasija, A.; Lisboa, G.; Luz, S.; Malley, J., Eds.; Cambridge University Press: Cambridge, UK and New York, NY, USA, 2022. DOI: 10.1017/9781009157926.
(6) Taarning, E.; Osmundsen, C. M.; Yang, X.; Voss, B.; Andersen, S. I.; Christensen, C. H. Zeolite-Catalyzed Biomass Conversion to Fuels and Chemicals. *Energy Environ. Sci.* **2011**, *4*, 793−804.
(7) Mardiana, S.; Azhari, N. J.; Ilmi, T.; Kadja, G. T. M. Hierarchical Zeolite for Biomass Conversion to Biofuel: A Review. *Fuel* **2022**, *309*, No. 122119.
(8) Ennaert, T.; Van Aelst, J.; Dijkmans, J.; De Clercq, R.; Schutyser, W.; Dusselier, M.; Verboekend, D.; Sels, B. F. Potential and Challenges of Zeolite Chemistry in the Catalytic Conversion of Biomass. *Chem. Soc. Rev.* **2016**, *45*, 584−611.
(9) Stanciakova, K.; Weckhuysen, B. M. Water−Active Site Interactions in Zeolites and Their Relevance in Catalysis. *Trends Chem.* **2021**, *3*, 456−468.
(10) Mei, D.; Lercher, J. A. Mechanistic Insights into Aqueous Phase Propanol Dehydration in H-ZSM-5 Zeolite. *AIChE J.* **2017**, *63*, 172−184.
(11) Mei, D.; Lercher, J. A. Effects of Local Water Concentrations on Cyclohexanol Dehydration in H-BEA Zeolites. *J. Phys. Chem. C* **2019**, *123*, 25255−25266.
(12) Zhi, Y.; Shi, H.; Mu, L.; Liu, Y.; Mei, D.; Camaioni, D. M.; Lercher, J. A. Dehydration Pathways of 1-Propanol on HZSM-5 in the Presence and Absence of Water. *J. Am. Chem. Soc.* **2015**, *137*, 15781−15794.
(13) Wang, Q.; Fan, H.; Wu, S.; Zhang, Z.; Zhang, P.; Han, B. Water as an Additive to Enhance the Ring Opening of Naphthalene. *Green Chem.* **2012**, *14*, 1152−1158.
(14) Chen, K.; Damron, J.; Pearson, C.; Resasco, D.; Zhang, L.; White, J. L. Zeolite Catalysis: Water Can Dramatically Increase or Suppress Alkane C-H Bond Activation. *ACS Catal.* **2014**, *4*, 3039−3044.
(15) Li, G.; Wang, B.; Resasco, D. E. Water-Mediated Heterogeneously Catalyzed Reactions. *ACS Catal.* **2020**, *10*, 1294−1309.
(16) Zecchina, A.; Bordiga, S.; Spoto, G.; Scarano, D.; Spanò, G.; Geobaldo, F. IR Spectroscopy of Neutral and Ionic Hydrogen-Bonded Complexes Formed upon Interaction of CH3OH, C2H5OH, (CH3)2O, (C2H5)2O and C4H8O with H-Y, H-ZSM-5 and H-Mordenite: Comparison with Analogous Adducts Formed on the H-Nafion Superacidic Membrane. *J. Chem. Soc., Faraday Trans.* **1996**, *92*, 4863−4875.
(17) Zygmunt, S. A.; Curtiss, L. A.; Iton, L. E.; Erhardt, M. K. Computational Studies of Water Adsorption in the Zeolite H-ZSM-5. *J. Phys. Chem. A* **1996**, *100*, 6663−6671.
(18) Jeanvoine, Y.; Ángyán, J. G.; Kresse, G.; Hafner, J. On the Nature of Water Interacting with Brønsted Acidic Sites. Ab Initio Molecular Dynamics Study of Hydrated HSAPO-34. *J. Phys. Chem. B* **1998**, *102*, 7307−7310.
(19) Wakabayashi, F.; Kondo, J. N.; Domen, K.; Hirose, C. FT-IR Study of H218O Adsorption on H-ZSM-5: Direct Evidence for the Hydrogen-Bonded Adsorption of Water. *J. Phys. Chem. A* **1996**, *100*, 1442−1444.
(20) Olson, D. H.; Zygmunt, S. A.; Erhardt, M. K.; Curtiss, L. A.; Iton, L. E. Evidence for Dimeric and Tetrameric Water Clusters in HZSM-5. *Zeolites* **1997**, *18*, 347−349.
(21) Krossner, M.; Sauer, J. Interaction of Water with Brønsted Acidic Sites of Zeolite Catalysts. Ab Initio Study of 1:1 and 2:1 Surface Complexes. *J. Phys. Chem. A* **1996**, *100*, 6199−6211.
(22) Vjunov, A.; Wang, M.; Govind, N.; Huthwelker, T.; Shi, H.; Mei, D.; Fulton, J. L.; Lercher, J. A. Tracking the Chemical Transformations at the Brønsted Acid Site upon Water-Induced Deprotonation in a Zeolite Pore. *Chem. Mater.* **2017**, *29*, 9030−9042.
(23) Wang, M.; Jaegers, N. R.; Lee, M. S.; Wan, C.; Hu, J. Z.; Shi, H.; Mei, D.; Burton, S. D.; Camaioni, D. M.; Gutiérrez, O. Y.; Glezakou, V. A.; Rousseau, R.; Wang, Y.; Lercher, J. A. Genesis and Stability of Hydronium Ions in Zeolite Channels. *J. Am. Chem. Soc.* **2019**, *141*, 3444−3455.
(24) Liu, P.; Mei, D. Identifying Free Energy Landscapes of Proton-Transfer Processes between Brønsted Acid Sites and Water Clusters Inside the Zeolite Pores. *J. Phys. Chem. C* **2020**, *124*, 22568−22576.
(25) Grifoni, E.; Piccini, G. M.; Lercher, J. A.; Glezakou, V. A.; Rousseau, R.; Parrinello, M. Confinement Effects and Acid Strength in Zeolites. *Nat. Commun.* **2021**, *12*, No. 2630.
(26) Smith, L.; Cheetham, A. K.; Morris, R. E.; Marchese, L.; Thomas, J. M.; Wright, P. A.; Chen, J. On the Nature of Water Bound to a Solid Acid Catalyst. *Science* **1996**, *271*, 799−802.
(27) Termath, V.; Haase, F.; Sauer, J.; Hutter, J.; Parrinello, M. Understanding the Nature of Water Bound to Solid Acid Surfaces. Ab Initio Simulation on HSAPO-34. *J. Am. Chem. Soc.* **1998**, *120*, 8512−8516.
(28) Kawai, Y.; Yamaguchi, S.; Okada, Y.; Takeuchi, K.; Yamauchi, Y.; Ozawa, S.; Nakai, H. Reactions of Protonated Water Clusters H +(H2O) n (n = 1−6) with Dimethylsulfoxide in a Guided Ion Beam Apparatus. *Chem. Phys. Lett.* **2003**, *377*, 69−73.
(29) Kletnieks, P. W.; Ehresmann, J. O.; Nicholas, J. B.; Haw, J. F. Adsorbate Clustering and Proton Transfer in Zeolites: NMR Spectroscopy and Theory. *ChemPhysChem* **2006**, *7*, 114−116.
(30) Cheng, H. P. Water Clusters: Fascinating Hydrogen-Bonding Networks, Solvation Shell Structures, and Proton Motion. *J. Phys. Chem. A* **1998**, *102*, 6201−6204.
(31) Wròblewski, T.; Ziemczonek, L.; Karwasz, G. P. Proton Transfer Reactions for Ionized Water Clusters. *Czech. J. Phys.* **2004**, *54*, 747−752.
(32) Stanciakova, K.; Louwen, J. N.; Weckhuysen, B. M.; Bulo, R. E.; Göltl, F. Understanding Water-Zeolite Interactions: On the Accuracy of Density Functionals. *J. Phys. Chem. C* **2021**, *125*, 20261−20274.

(33) Zygmunt, S. A.; Curtiss, L. A.; Iton, L. E. Protonation of an H2O Dimer by a Zeolitic Brønsted Acid Site. *J. Phys. Chem. B* **2001**, *105*, 3034−3038.
(34) Vener, M. V.; Rozanska, X.; Sauer, J. Protonation of Water Clusters in the Cavities of Acidic Zeolites: (H2O)N·H-Chabazite, n = 1−4. *Phys. Chem. Chem. Phys.* **2009**, *11*, 1702−1712.
(35) Ison, A.; Gorte, R. J. The Adsorption of Methanol and Water on H-ZSM-5. *J. Catal.* **1984**, *89*, 150−158.
(36) Jentys, A.; Warecka, G.; Derewinski, M.; Lercher, J. A. Adsorption of Water on ZSM5 Zeolites. *J. Phys. Chem. A* **1989**, *93*, 4837−4843.
(37) Pelmenschikov, A. G.; van Wolput, J. H. M. C.; Jaenchen, J.; van Santen, R. A. (A,B,C) Triplet of Infrared OH Bands of Zeolitic H-Complexes. *J. Phys. Chem. A* **1995**, *99*, 3612−3617.
(38) Pelmenschikov, A. G.; Van Santen, R. A. Water Adsorption on Zeolites: Ab-Initio Interpretation of IR Data. *J. Phys. Chem. A* **1993**, *97*, 10678−10680.
(39) Mihaleva, V. V.; Van Santen, R. A.; Jansen, A. P. J. Quantum Chemical Calculation of Infrared Spectra of Acidic Groups in Chabazite in the Presence of Water. *J. Chem. Phys.* **2004**, *120*, 9212−9221.
(40) Zecchina, A.; Geobaldo, F.; Spoto, G.; Bordiga, S.; Ricchiardi, G.; Buzzoni, R.; Petrini, G. FTIR Investigation of the Formation of Neutral and Ionic Hydrogen-Bonded Complexes by Interaction of H-ZSM-5 and H-Mordenite with CH3CN and H2O: Comparison with the H-NAFION Superacidic System. *J. Phys. Chem. A* **1996**, *100*, 16584−16599.
(41) Bonn, M.; Van Santen, R. A.; Lercher, J. A.; Kleyn, A. W.; Bakker, H. J. Picosecond Infrared Activation of Methanol in Acid Zeolites. *Chem. Phys. Lett.* **1997**, *278*, 213−219.
(42) Bonn, M.; Brugmans, M. J. P.; Kleyn, A. W.; Van Santen, R. A. Fast Energy Delocalization upon Vibrational Relaxation of a Deuterated Zeolite Surface Hydroxyl. *J. Chem. Phys.* **1995**, *102*, 2181−2186.
(43) Hack, J. H.; Dombrowski, J. P.; Ma, X.; Chen, Y.; Lewis, N. H. C.; Carpenter, W. B.; Li, C.; Voth, G. A.; Kung, H. H.; Tokmakoff, A. Structural Characterization of Protonated Water Clusters Confined in HZSM-5 Zeolites. *J. Am. Chem. Soc.* **2021**, *143*, 10203−10213.
(44) Donaldson, P. M.; Howe, R. F.; Hawkins, A. P.; Towrie, M.; Greetham, G. M. Ultrafast 2D-IR Spectroscopy of Intensely Optically Scattering Pelleted Solid Catalysts. *J. Chem. Phys.* **2023**, *158*, No. 114201.
(45) Yamada, S. A.; Shin, J. Y.; Thompson, W. H.; Fayer, M. D. Water Dynamics in Nanoporous Silica: Ultrafast Vibrational Spectroscopy and Molecular Dynamics Simulations. *J. Phys. Chem. C* **2019**, *123*, 5790−5803.
(46) Li, C.; Swanson, J. M. J. Understanding and Tracking the Excess Proton in Ab Initio Simulations; Insights from IR Spectra. *J. Phys. Chem. B* **2020**, *124*, 5696−5708.
(47) Li, C.; Voth, G. A. Using Constrained Density Functional Theory to Track Proton Transfers and to Sample Their Associated Free Energy Surface. *J. Chem. Theory Comput.* **2021**, *17*, 5759−5765.
(48) Kim, J.; Schmitt, U. W.; Gruetzmacher, J. A.; Voth, G. A.; Scherer, N. E. The Vibrational Spectrum of the Hydrated Proton: Comparison of Experiment, Simulation, and Normal Mode Analysis. *J. Chem. Phys.* **2002**, *116*, 737−746.
(49) Yu, Q.; Carpenter, W. B.; Lewis, N. H. C.; Tokmakoff, A.; Bowman, J. M. High-Level VSCF/VCI Calculations Decode the Vibrational Spectrum of the Aqueous Proton. *J. Phys. Chem. B* **2019**, *123*, 7214−7224.
(50) Headrick, J. M.; Diken, E. G.; Walters, R. S.; Hammer, N. I.; Christie, R. A.; Cui, J.; Myshakin, E. M.; Duncan, M. A.; Johnson, M. A.; Jordan, K. D. Spectral Signatures of Hydrated Proton Vibrations in Water Clusters. *Science* **2005**, *308*, 1765−1769.
(51) Schmidt, J. R.; Corcelli, S. A.; Skinner, J. L. Pronounced Non-Condon Effects in the Ultrafast Infrared Spectroscopy of Water. *J. Chem. Phys.* **2005**, *123*, No. 044513.
(52) Bordiga, S.; Lamberti, C.; Bonino, F.; Travert, A.; Thibault-Starzyk, F. Probing Zeolites by Vibrational Spectroscopies. *Chem. Soc. Rev.* **2015**, *44*, 7262−7341.
(53) Edler, J.; Hamm, P. Two-Dimensional Vibrational Spectroscopy of the Amide I Band of Crystalline Acetanilide: Fermi Resonance, Conformational Substates, or Vibrational Self-Trapping? *J. Chem. Phys.* **2003**, *119*, 2709−2715.
(54) Brunauer, S.; Emmett, P. H.; Teller, E. Adsorption of Gases in Multimolecular Layers. *J. Am. Chem. Soc.* **1938**, *60*, 309−319.
(55) Olson, D. H.; Haag, W. O.; Borghard, W. S. Use of Water as a Probe of Zeolitic Properties: Interaction of Water with HZSM-5. *Microporous Mesoporous Mater.* **2000**, *35*−*36*, 435−446.
(56) Eckstein, S.; Hintermeier, P. H.; Zhao, R.; Baráth, E.; Shi, H.; Liu, Y.; Lercher, J. A. Influence of Hydronium Ions in Zeolites on Sorption. *Angew. Chem., Int. Ed.* **2019**, *58*, 3450−3455.
(57) Bolis, V.; Busco, C.; Ugliengo, P. Thermodynamic Study of Water Adsorption in High-Silica Zeolites. *J. Phys. Chem. B* **2006**, *110*, 14849−14859.
(58) Keenan, J. H.; Keyes, F. G.; Hill, P. G.; Moore, J. G. *Steam Tables*; Wiley: New York, 1969.
(59) Gillan, M. J.; Alfè, D.; Michaelides, A. Perspective: How Good Is DFT for Water? *J. Chem. Phys.* **2016**, *144*, No. 130901.
(60) Ruiz Pestana, L.; Mardirossian, N.; Head-Gordon, M.; Head-Gordon, T. Ab Initio Molecular Dynamics Simulations of Liquid Water Using High Quality Meta-GGA Functionals. *Chem. Sci.* **2017**, *8*, 3554−3565.
(61) Marsalek, O.; Markland, T. E. Quantum Dynamics and Spectroscopy of Ab Initio Liquid Water: The Interplay of Nuclear and Electronic Quantum Effects. *J. Phys. Chem. Lett.* **2017**, *8*, 1545−1551.
(62) Ohto, T.; Dodia, M.; Xu, J.; Imoto, S.; Tang, F.; Zysk, F.; Kühne, T. D.; Shigeta, Y.; Bonn, M.; Wu, X.; Nagata, Y. Accessing the Accuracy of Density Functional Theory through Structure and Dynamics of the Water-Air Interface. *J. Phys. Chem. Lett.* **2019**, *10*, 4914−4919.
(63) Bell, R. J.; Dean, P. Atomic Vibrations in Vitreous Silica. *Discuss. Faraday Soc.* **1970**, *50*, 55−61.
(64) Thouless, D. J. Electrons in Disordered Systems and the Theory of Localization. *Phys. Rep.* **1974**, *13*, 93−142.
(65) Schmitt, U. W.; Voth, G. A. The Computer Simulation of Proton Transport in Water. *J. Chem. Phys.* **1999**, *111*, 9361.
(66) Wu, Y.; Chen, H.; Wang, F.; Paesani, F.; Voth, G. A. An Improved Multistate Empirical Valence Bond Model for Aqueous Proton Solvation and Transport. *J. Phys. Chem. B* **2008**, *112*, 476−482.
(67) Biswas, R.; Tse, Y.-L. S.; Tokmakoff, A.; Voth, G. A. Role of Presolvation and Anharmonicity in Aqueous Phase Hydrated Proton Solvation and Transport. *J. Phys. Chem. B* **2016**, *120*, 1793−1804.
(68) Kaduk, B.; Kowalczyk, T.; Van Voorhis, T. Constrained Density Functional Theory. *Chem. Rev.* **2012**, *112*, 321−370.
(69) Widjaja, E.; Garland, M. Pure Component Spectral Reconstruction from Mixture Data Using SVD, Global Entropy Minimization, and Simulated Annealing. Numerical Investigations of Admissible Objective Functions Using a Synthetic 7-Species Data Set. *J. Comput. Chem.* **2002**, *23*, 911−919.
(70) Carpenter, W. B.; Fournier, J. A.; Biswas, R.; Voth, G. A.; Tokmakoff, A. Delocalization and Stretch-Bend Mixing of the HOH Bend in Liquid Water. *J. Chem. Phys.* **2017**, *147*, No. 084503.
(71) Carpenter, W. B.; Fournier, J. A.; Lewis, N. H. C.; Tokmakoff, A. Picosecond Proton Transfer Kinetics in Water Revealed with Ultrafast IR Spectroscopy. *J. Phys. Chem. B* **2018**, *122*, 2792−2802.
(72) Bloem, R.; Garrett-Roe, S.; Strzalka, H.; Hamm, P.; Donaldson, P. Enhancing Signal Detection and Completely Eliminating Scattering Using Quasi-Phase-Cycling in 2D IR Experiments. *Opt. Express* **2010**, *18*, 27067−27078.
(73) Olson, D. H.; Khosrovani, N.; Peters, A. W.; Toby, B. H. Crystal Structure of Dehydrated CsZSM-5 (5.8Al): Evidence for Nonrandom Aluminum Distribution. *J. Phys. Chem. B* **2000**, *104*, 4844−4848.

https://doi.org/10.1021/acs.jpcc.3c03611
J. Phys. Chem. C 2023, 127, 16175−16186

(74) Zhang, Y.; Yang, W. Comment on "Generalized Gradient Approximation Made Simple.". *Phys. Rev. Lett.* **1998**, *80*, 890.
(75) Kühne, T. D.; Laino, T.; Iannuzzi, M.; Ben, M. D.; Khaliullin, R. Z.; Schütt, O.; Rybkin, V. V.; Seewald, P.; Schiffmann, F.; Golze, D.; Schade, R.; Mundy, C. J.; Chulkov, S.; et al. CP2K: An Electronic Structure and Molecular Dynamics Software Package - Quickstep: Efficient and Accurate Electronic Structure Calculations. *J. Chem. Phys.* **2020**, *152*, No. 194103.
(76) VandeVondele, J.; Krack, M.; Mohamed, F.; Parrinello, M.; Chassaing, T.; Hutter, J. QUICKSTEP: Fast and Accurate Density Functional Calculations Using a Mixed Gaussian and Plane Waves Approach. *Comput. Phys. Commun.* **2005**, *167*, 103−128.
(77) Lippert, G.; Hutter, J.; Parrinello, M. The Gaussian and Augmented-Plane-Wave Density Functional Method for Ab Initio Molecular Dynamics Simulations. *Theor. Chem. Acc.* **1999**, *103*, 124−140.
(78) Goedecker, S.; Teter, M.; Hutter, J. Separable Dual-Space Gaussian Pseudopotentials. *Phys. Rev. B* **1996**, *54*, 1703−1710.
(79) Grimme, S.; Antony, J.; Ehrlich, S.; Krieg, H. A Consistent and Accurate Ab Initio Parameterization of Density Functional Dispersion Correctin (DFT-D) for the 94 Elements of H-Pu. *J. Chem. Phys.* **2010**, *132*, No. 154104.

https://doi.org/10.1021/acs.jpcc.3c03611
J. Phys. Chem. C 2023, 127, 16175−16186